

Figure S1. Cell growth curve analysis and morphology defects. Related to Figure 1.

(A-E) Growth curves for wildtype and mutant strains. Cells were grown in YEPD at 25°C or 34°C, as indicated, with shaking in a microplate absorbance reader. OD₆₀₀ was measured at 5 min intervals. Data averaged from ≥ 18 duplicates/strain. Lines represent averages, and surrounding shading represents SEM. (F) Bnr1-GFP average signal distribution across the cell length (back of mother cell to bud tip) in wildtype and *bni1*Δ cells. Data averaged from 50 cells per strain. (G) Average mother cell area ($n \geq 50$ cells per strain). (H) Average total fluorescence of actin cable staining (Alexa-488 phalloidin) in fixed cells ($n = 10$ cells per strain). (I) Fluorescence intensity (thickness) of individual actin cables measured by line scan analysis in the same mother cells as in H ($n > 25$ cables per strain). Black line, mean. Student's T-test used to determine the indicated significant difference ($p < 0.05$) from the wildtype ('w'), appropriate tropomyosin single mutant ('t'), or appropriate formin single mutant ('f') strain.

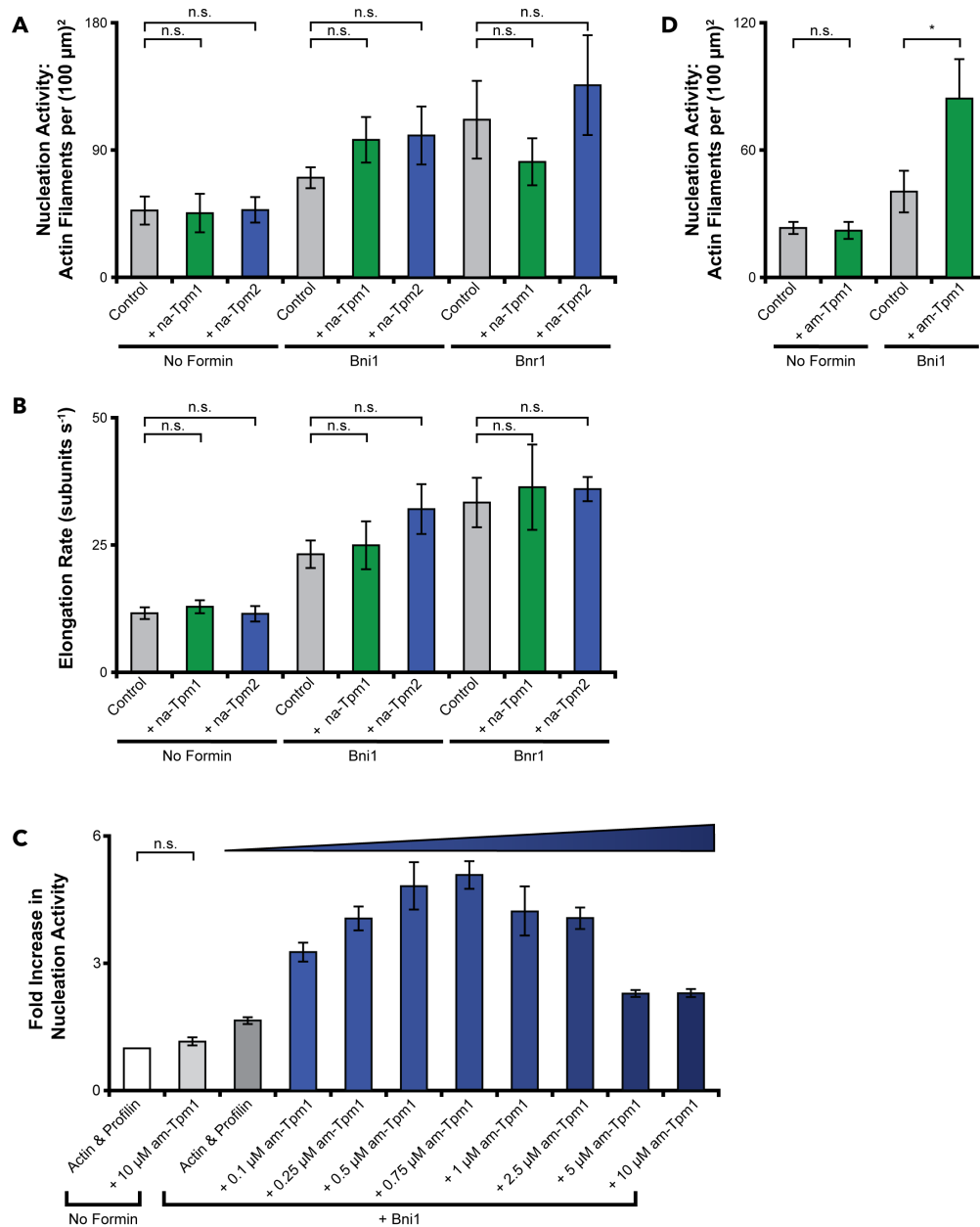


Figure S2. Effects of na-Tpm1 and na-Tpm2 on actin filament nucleation and elongation rates in the presence or absence of formins. Related to Figure 3.

(A) Actin nucleation effects determined by in vitro TIRF microscopy. Reactions contained 1 μM monomeric actin (20% Oregon Green-labeled), 3 μM yeast profilin and variable components: 250 pM Bni1, 200 pM Bnr1, 2.5 μM na-Tpm1, and 2.5 μM na-Tpm2. Number of filaments per FOV was quantified 5 min after initiation of actin assembly. Data averaged from two independent experiments (6 FOV per condition). (B) Actin filament elongation rates determined from the same reactions as in A, calculated from the slopes of individual filament traces, length versus time ($n \geq 30$ filaments per condition). (C) Concentration-dependent effects of am-Tpm1 on Bni1-mediated actin nucleation. TIRF microscopy reactions as above but with variable concentrations of am-Tpm1. Data averaged from three independent experiments (6 FOV per condition). (D) Effects of am-Tpm1 on Bni1-mediated actin nucleation using yeast actin by TIRF microscopy. Reactions as above except using yeast actin as the unlabeled actin component. Data averaged from two independent experiments (6 FOV per condition). Error bars, SEM. Student's T-test used to determine significant differences: n.s. – not significant, * < 0.05 .

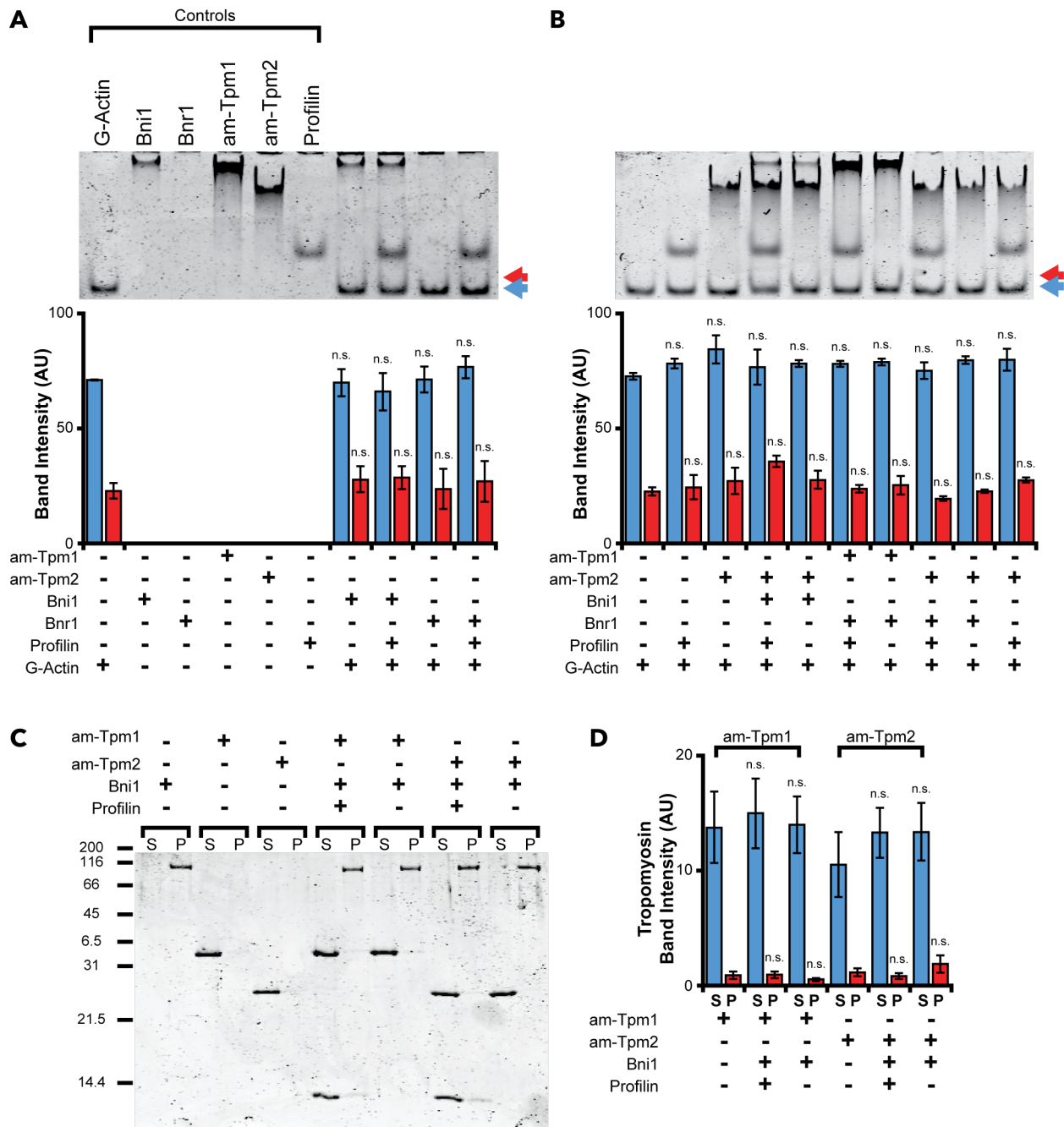


Figure S3. Formin-tropomyosin interactions are specific to Bni1 and Tpm1. Related to Figure 4.

(A-B) Native gel shift analysis to detect stable complexes with G-actin. Reactions containing one of more of the following components, as indicated: 1.0 μ M G-actin, 0.5 μ M Bni1, 0.5 μ M Bnr1, 5.0 μ M am-Tpm1, 5.0 μ M am-Tpm2, or 3 μ M yeast profilin (Pfy1). Reactions were fractionated by native PAGE, and gels were stained with Coomassie Blue. G-actin band intensity was quantified at the unshifted (blue arrow) and shifted (red arrow) positions. Data averaged from two independent experiments and plotted for each position (blue and red, as above). Significant differences are compared to actin alone control (Lane 1). Note that Bnr1 is absent from the gel lanes, because it migrates out of the gel (towards the anode). (C) Representative gel of supernatant and pellet fractions from pull-down assays to detect binding between 0.5 μ M Bni1 (on beads) and 5 μ M am-Tpm1 or am-Tpm2 in the presence or absence of profilin. (D) Quantification of the amount of tropomyosin in the supernatant and pellet fractions from gels in C. Significant difference is determined compared to the tropomyosin alone condition. Error bars, SEM. Student's T-test used to determine significant differences, n.s. – not significant.

Supplemental Experimental Procedures

Reagents

All reagents were purchased from Sigma-Aldrich, St. Louis, MO, unless otherwise noted.

Plasmid construction

The vectors for expression of hexa-histidine (6× HIS)-Bni1 (residues 1227-1953) and 6× HIS-Bnr1 (residues 757-1375) in *S. cerevisiae* were described previously [S1, S2]. Wildtype yeast *TPM1* and *TPM2* ORFs were PCR amplified from yeast genomic DNA and subcloned into the pET-DUET1 *E. coli* expression vector using NcoI and NotI. By a similar strategy, we constructed plasmids for expression and purification of ‘acetylation-mimetic’ (am) versions of Tpm1 and Tpm2 (am-Tpm1 and am-Tpm2) with an N-terminal Met-Ala-Ser extension to mimic acetylation of the N-terminal Met [S3].

Yeast strain construction

Unless otherwise noted, all strains are in the s288c background isogenic to DDY902 (*MATa*, *his3Δ200*, *leu2-3,112*, *ura3-52*, *ade2-1*) or DDY904 (*MATa*, *his3Δ200*, *leu2-3,112*, *ura3-52*, *lys-801*) [S4]. Mutant yeast strains *tpm1Δ::KANMX6* (SAY044), *tpm2Δ::KANMX6* (SAY045), *bnr1Δ::HISM3* (SAY046), and *bni1Δ::HISM3* (SAY047) were generated by homologous recombination using either a *KANMX6* or *HISM3* cassette [S5]. Knockouts were confirmed by PCR analysis of isolated genomic DNA. Double mutants were generated by crossing single mutants above, sporulating diploids, dissecting tetrads, genotyping, and confirming mutations by PCR.

Protein purification

Rabbit skeletal muscle actin [S6] and Oregon Green-labeled actin [S7] were purified as described, and the concentration and degree of labeling of OG-actin was determined as described. Bni1 FH1-FH2-C and Bnr1 FH1-FH2-C [S8] and wildtype and mutant yeast profilins (Pfy1, Pfy1-4, and Pfy1-19) were purified as described [S1]. Full-length acetylation-mimetic (am) and non-acetylated Tpm1 and Tpm2 proteins were expressed and purified from *E. coli* as described [S3]. Briefly, plasmids were transformed into *E. coli* strain BL21 DE3, and 2 L cultures of cells were grown at 37°C to OD600 = 1.0, then induced with 0.4 mM IPTG for 4 h. Cells were harvested by centrifugation, washed once with 1× PBS, pelleted, and stored at -80°C until use. Each cell pellet, corresponding to 1 L of culture, was resuspended in 40 mL lysis buffer (20 mM Tris pH 7.5, 100 mM NaCl, 2mM EDTA) and lysed by sonication. The crude cell lysate was incubated in an 80°C water bath for 10 min, and then cleared by centrifugation for 20 min at 29,000 × g. Tropomyosin was isoelectrically precipitated by adjusting the pH to 4.5 using a stock of 0.3 M HCl. After 15 min, the tropomyosin was pelleted by centrifugation for 20 min at 29,000 × g, resuspended in 50 mL running buffer (10 mM phosphate pH 7.0, 100 mM NaCl), and adjusted to pH 7.0 using a stock of 1 M NaOH. Tropomyosin was further purified by anion exchange chromatography on a HiTrap Q HP column (GE Healthcare, Pittsburgh, PA) equilibrated in running buffer, and eluted with a gradient of 100-400 mM KCl. Peak fractions were pooled, dialyzed into HEK buffer (20 mM Hepes pH 7.5, 1 mM EDTA, 50 mM KCl), and stored at 4°C for up to 6 months.

Cell imaging

To assess actin organization, yeast cells were fixed and stained with fluorescently labeled phalloidin as described [S9]. Briefly, strains were grown in yeast extract/peptone/2% glucose (YEPD) at 25°C to early/mid log phase and fixed at room temperature with 4.5% formaldehyde for 60 min. Then cells were stained overnight at 4°C with Alexafluor-488-phalloidin and washed three times with PBS before imaging. Cells were imaged in mounting media (10 mM NaPO₄, pH 7.4, 75 mM NaCl, 4.3 mM p-phenylenediamine, 0.01 mg/mL 4'-diamidino-2-phenylindole, and 45% glycerol) on an upright Zeiss Axioskop2 mot plus microscope (Zeiss, Peabody, MA) equipped with a 100× Plan-Apochromat oil immersion objective (NA 1.4; Zeiss), and images were captured using a Hamamatsu digital charge-coupled device (CCD) camera (Hamamatsu Photonics, Bridgewater, NJ). Single focal plane images were acquired using Openlab software (PerkinElmer, Waltham, MA). Number of actin cables in mother cells was manually scored from single focal plane images in ImageJ (Fig. 1D). Total actin cable fluorescence intensity in mother cells was quantified in ImageJ after boxing and subtracting the fluorescence of any actin patches (Fig. S1H). Thickness of individual actin cables in the same mother cells as above was quantified by line scan analysis in ImageJ, measuring peak fluorescence intensity (Fig. S1I). To assess GFP-Sec4 distribution between mother and bud compartments, yeast strains were transformed with a URA3-marked CEN plasmid expressing GFP-Sec4 and grown in synthetic medium (2% glucose) lacking uracil to early/mid log phase (OD600 = 0.1-0.4). Live cells were then imaged on a Nikon Ni-E upright microscope (Nikon Instruments, New York, NY) equipped with a 100× Apo oil

immersion objective (NA 1.45; Nikon Instruments), a spinning disk head (CSU-W1; Yokogawa Corporation of America, Sugar Land, TX), and an electron-multiplying charge-coupled device (EMCCD) camera (iXon 897U; Andor Technology, Belfast, Northern Ireland). Images were acquired using Elements AR software (Nikon). Z-series were collected (0.2- μm step size; 100 ms exposure for each step). GFP-Sec4 fluorescence levels in the bud and mother compartments were measured using ImageJ, and used to calculate the ratio of fluorescence in the bud to mother (Fig. 2B). The mother compartment area was also measured in ImageJ for the same strains (Fig. 2C).

Total internal reflection fluorescence (TIRF) microscopy

Glass coverslips (24 \times 60 mm #1.5; Fisher Scientific, Pittsburg, PA) were sonicated for 1 h in 2% Micro-90 detergent, followed by 1 h sonication in 100% ethanol, then 30 min sonication in 0.1 M KOH and ddH₂O, respectively. Cleaned coverglass was stored in 100% ethanol before use. Prior to imaging, each coverslip was rinsed with ddH₂O, dried with N₂, and coated by applying 120 μL of 2 mg/mL methoxy-poly(ethylene glycol) (mPEG)-silane MW 2,000 (Laysan Bio, Arab, AL) and 4 $\mu\text{g}/\text{mL}$ biotin-PEG-silane MW 3,400 (Laysan Bio, Arab, AL) resuspended in 80% ethanol, pH 2.0. Coated coverslips were incubated 16 h at 70°C. Flow cells were assembled by rinsing PEG-coated coverslips with ddH₂O, drying with N₂, and adhering to μ -Slide VI0.1 (0.1 mm \times 17 mm \times 1 mm) flow chambers (Ibidi, Martinsried, Germany) with double-sided tape (2.5 cm \times 2 mm \times 120 μm) sealed with five-minute epoxy resin (Devcon, Riviera Beach, FL). Flow cells were incubated for 1 min with 1% BSA, then incubated for 1 min with TIRF buffer (10 mM imidazole pH 7.4, 50 mM KCl, 1 mM MgCl₂, 1 mM EGTA, 0.2 mM ATP, 10 mM DTT, 15 mM glucose, and 0.25% methyl cellulose [4000 cP]). TIRF reactions were initiated by adding 1 μM actin (20% OG-labeled) to premixed actin-binding proteins. Reactions were introduced into the flow chamber, which was then mounted on the microscope stage for imaging. Time between addition of actin and the start of TIRF recording was 180 s. Time lapse imaging was performed on a Nikon-Ti200 inverted microscope (Nikon Instruments) equipped with a 488 nm argon laser (150 mW; Melles Griot, Carlsbad, CA), a 60 \times Apo oil-immersion TIRF objective (NA 1.49; Nikon Instruments), and an EMCCD camera with a pixel size of 0.267 μm (Andor), and running NIS-Elements (Nikon Instruments). Focus was maintained by the Perfect Focus system (Nikon Instruments). Images were collected at 5 s intervals for 10 min. Background fluorescence was removed from each image in a stack using the background subtraction tool (rolling ball radius, 50 pixels) in ImageJ. Minimal contrast enhancement or changes to the black level were applied to entire stack to improve image quality for analysis and display. Filament nucleation events were scored 300 s after the initiation of each reaction for ≥ 12 fields of view from \geq two independent reactions. Baseline nucleation levels varied between experiments due to batch-specific and age-dependent differences in the nucleation activity of actin monomer column fractions, gel-filtered every two weeks. For this reason, nucleation effects by specific proteins (e.g., Bni1 and Tpm1) were assessed as fold increase over control for each experiment. Filament elongation rates were determined from $n \geq 30$ filaments from each of three independent reactions. Filament length was measured using the freehand line tool in ImageJ for filaments that could be tracked for 300 s. Elongation rates were determined by plotting filament length versus time, where the rate is the slope. To express rates in actin subunits s⁻¹, we used the conversion factor of 374 subunits per micron of F-actin.

Native gel shift assays

For native PAGE assays, 1 μM Ca-ATP-G-actin and 1.2 μM Latrunculin B were incubated for 10 min in 1 \times loading buffer (25 mM Tris pH 7.5, 200 mM glycine, 0.2 mM ATP, 0.6 mM CaCl₂, 0.2 mM DTT, and 5% glycerol) with other proteins as indicated: Bni1 or Bnr1 (0.5 μM), am-Tpm1 or am-Tpm2 (5 μM), and/or yeast profilin (3 μM). Reactions were analyzed on 7.5% native gels, run for 90 min at 100 mV, and then stained with Coomassie Blue. Actin band intensities in specific positions were measured using ImageJ for the analysis in Figure 4E and Figure S3A & S3B. Background staining in the gels was controlled for using the background subtraction tool (rolling ball radius, 50 pixels).

Pull-down binding assays

Binding of 6His-Bni1 (FH1-FH2-C) (0.5 μM) to am-Tpm1 or am-Tpm2 (2.5 μM) in the presence and absence of yeast profilin (3 μM) was assessed by pull-down assays. Proteins were incubated together in 25 μL reactions for 10 min at room temperature, then 5 μL NiNTA agarose beads was added, and reactions were incubated for another 10 min. Beads were pelleted and washed once in 25 μL HEK buffer. Supernatants and pellet fractions were analyzed on Coomassie-stained gels (Fig S3C), and bands intensities were quantified in ImageJ (Fig S3D).

Supplemental References

- S1. Moseley, J.B., Sagot, I., Manning, A.L., Xu, Y., Eck, M.J., Pellman, D., and Goode, B.L. (2004). A conserved mechanism for Bni1- and mDial-induced actin assembly and dual regulation of Bni1 by Bud6 and profilin. *Mol Biol Cell* *15*, 896-907.
- S2. Moseley, J.B., and Goode, B.L. (2005). Differential activities and regulation of *Saccharomyces cerevisiae* formin proteins Bni1 and Bnr1 by Bud6. *J Biol Chem* *280*, 28023-28033.
- S3. Maytum, R., Geeves, M.A., and Konrad, M. (2000). Actomyosin regulatory properties of yeast tropomyosin are dependent upon N-terminal modification. *Biochemistry* *39*, 11913-11920.
- S4. Kozminski, K.G., Chen, A.J., Rodal, A.A., and Drubin, D.G. (2000). Functions and functional domains of the GTPase Cdc42p. *Mol Biol Cell* *11*, 339-354.
- S5. Longtine, M.S., McKenzie, A., 3rd, Demarini, D.J., Shah, N.G., Wach, A., Brachat, A., Philippsen, P., and Pringle, J.R. (1998). Additional modules for versatile and economical PCR-based gene deletion and modification in *Saccharomyces cerevisiae*. *Yeast* *14*, 953-961.
- S6. Spudich, J.A., and Watt, S. (1971). The regulation of rabbit skeletal muscle contraction. I. Biochemical studies of the interaction of the tropomyosin-troponin complex with actin and the proteolytic fragments of myosin. *J Biol Chem* *246*, 4866-4871.
- S7. Kuhn, J.R., and Pollard, T.D. (2005). Real-time measurements of actin filament polymerization by total internal reflection fluorescence microscopy. *Biophys J* *88*, 1387-1402.
- S8. Moseley, J.B., Maiti, S., and Goode, B.L. (2006). Formin proteins: purification and measurement of effects on actin assembly. *Methods Enzymol* *406*, 215-234.
- S9. Graziano, B.R., Jonasson, E.M., Pullen, J.G., Gould, C.J., and Goode, B.L. (2013). Ligand-induced activation of a formin-NPF pair leads to collaborative actin nucleation. *J Cell Biol* *201*, 595-611.